

## A study on the background and clustering seismicity in the Taiwan region by using point process models

Jiancang Zhuang,<sup>1</sup> Chung-Pai Chang,<sup>2</sup> Yosihiko Ogata,<sup>1</sup> and Yuh-Ing Chen<sup>3</sup>

Received 28 April 2004; revised 5 February 2005; accepted 14 March 2005; published 7 May 2005.

[1] This paper investigates the shallow seismicity occurring in the Taiwan region during the 20th century using a stochastic declustering method that has been developed on the basis of the theory of the epidemic-type aftershock sequence model. It provides a probability based tool to objectively separate the space-time occurrences of earthquakes into a background and a clustering component. On the basis of the background and clustering seismicity rates, we discuss the correlation between the distribution of the cluster ratio and the regional seismotectonic structures. Specifically, we find that the areas of the highest clustering ratio correspond to the major strike-slip fault traces in and around Taiwan. Additionally, in the Taiwan inland region, during the period 1960–1990, the outputs for the stochastically declustered catalogue show a clear quiescence in background seismicity preceding the recovery of activation and the occurrences of the 1999 Chi-Chi earthquake of  $M_L$ 7.3, while the other active regions show stationary background activity. This could be interpreted as an effect of the aseismic slip in the Chi-Chi rupture fault, whereby the inland region around the Chi-Chi source becomes a stress shadow.

**Citation:** Zhuang, J., C.-P. Chang, Y. Ogata, and Y.-I. Chen (2005), A study on the background and clustering seismicity in the Taiwan region by using point process models, *J. Geophys. Res.*, 110, B05S18, doi:10.1029/2004JB003157.

### 1. Introduction

[2] Taiwan is located on the convergent boundary between the Eurasian and the Philippine plates, and is one of the most active seismic regions in the world. In the 20th century, disastrous earthquakes in this region have caused great damage to properties, as well as to human lives [see, e.g., Hsu, 1961; Tsai, 1985; Wang and Kuo, 1995; Wang, 1998]. It is thus important to recognize background seismicity in the Taiwan region for the purposes of future earthquake hazard evaluation. In addition to main shocks, large aftershocks may also pose significant hazards, especially in populated areas where buildings have already been weakened by the main shock, which is one of the reasons why it is important to assess seismic damage caused by both main shocks and aftershocks. In order to estimate potential hazards caused by background seismicity, and to characterize earthquake clusters, a proper separation of background seismicity from total seismicity is necessary.

[3] In section 2, we present the motivation for proposing a probability-based declustering method, and then give a brief description of the space-time ETAS model and the

stochastic declustering method. In section 3, we consider the tectonic background of the Taiwan region and henceforth discuss our data selection. In sections 4–7, we use the model-based declustering method as a basic tool through which to obtain background seismicity and clustering seismicity in the Taiwan region, during the period 1900–1999, and hence describe their relation to the seismotectonic features in various important subregions in Taiwan. We also discuss temporal seismicity rate changes during the century, with special reference to the 1999 Chi-Chi earthquake.

### 2. Modeling

#### 2.1. Why Stochastic Declustering

[4] Declustering is one of the most important and frequently discussed issues in the study of seismicity. Seismicity is known to be clustered in both space and time, with earthquake clusters complicating statistical analysis of the seismic background variation that might be related to the stress changes in the tectonic environments. Moreover, the overlap of these clusters causes difficulties in the analysis of these clusters themselves. On the other hand, however, there is a great need for intensive study into earthquake clusters. For the purpose of long-term earthquake prediction, a good estimate of the background seismicity rate is necessary, with temporal and spatial clustering in the earthquake catalogue removed.

[5] Earthquake cluster features differ from place to place, and give different impressions to seismologists, who have thus proposed a number of declustering methods. These

<sup>1</sup>Institute of Statistical Mathematics, Tokyo, Japan.

<sup>2</sup>Center for Space and Remote Sensing Research, National Central University, Jhongli City, Taiwan.

<sup>3</sup>Institute of Statistics, National Central University, Chung-li, Taiwan.

methods can be classified into two classes: window based and link based. The window-based methods decluster an earthquake catalogue by removing the smaller earthquakes in a space-time window around a larger event (identified as the main shock) [see, e.g., *Utsu, 1969; Gardner and Knopoff, 1974*]. Usually, the larger the magnitude of the main shock, the bigger the window size. The link-based methods remove events which are within a compromised space-time distance to an earlier event [*Resenberg, 1985*] (for single-link clusters, see, *Frohlich and Davis [1990]* and *Davis and Frohlich [1991]*).

[6] In these conventional declustering methods, it is difficult to find optimal parameters for the sizes of space-time windows or the link distance and, as such, these are often chosen on the basis of the researcher's experience. Thus the declustering output may be quite sensitive to such subjective choices, which is one of the reasons why there have been so many declustering methods. Another reason for the existence of so many declustering methods is that uncertainty over underground earthquake processes usually results in a lack of clarity over the concept of an aftershock.

[7] Another shortcoming of conventional declustering is that removing earthquakes in the catalogue may cause losses of potentially useful information. A more suitable way is therefore to use a model which quantifies the observed data and then to use these quantified observations to test the hypotheses on seismicity and to evaluate its confidence level.

[8] Most of the statistical models for the space-time-magnitude occurrences of earthquake clusters are in the form of branching point process [*Kagan, 1991; Musmeci and Vere-Jones, 1992; Rathbun, 1993; Ogata, 1998; Ogata et al., 2003; Ogata, 2004; Zhuang et al., 2002, 2004; Console and Murru, 2001; Console et al., 2003*]. In general, these models classify seismicity into two components, the background and the cluster, where each earthquake event, whether it be from the background component (usually assumed to be a space-time Poisson process, stationary or nonstationary, homogeneous or nonhomogeneous) or generated by another event, produces (triggers) its own offspring (aftershocks) according to some branching rules. In the models mentioned above, *Musmeci and Vere-Jones [1992]*, *Ogata [1998]*, *Zhuang et al. [2002, 2004]*, and *Console et al. [2003]* consider the use of spatially inhomogeneous background rates in the model. *Musmeci and Vere-Jones [1992]* assume that the background seismicity was proportional to a kernel estimate obtained from spatial locations of all the earthquakes, including clusters. *Ogata [1998]* uses a conventional declustering method to provide a preliminary estimate of the background rate, fitting bicubic B spline functions before fitting it to the model. *Console et al. [2003]* first divided the study region into many cells, then set the smoothed values at each node by averaging the number of events in the neighboring cells. To avoid presetting the background rate, *Zhuang et al. [2002, 2004]* use an iterative approach to simultaneously estimate the background seismicity rate and the parameters associated with the clustering structures, where the background seismicity rate is estimated by weighted variable kernel functions. An alternative is to use

Bayesian analysis with smoothness prior for the background rates as well as for other parameters [*Ogata et al., 2003; Ogata, 2004*].

[9] To obtain an objectively declustered catalogue, *Zhuang et al. [2002, 2004]* propose a stochastic declustering method as an alternative to the conventional methods. In this method, it is no longer determined whether an earthquake is a background event or if it is triggered by another. Instead, each event has a probability of being either a background event or a direct offspring triggered by others. The main task of the stochastic declustering algorithm is then to estimate this probability for each event, according to some models used to describe earthquake clustering features.

## 2.2. Space-Time Epidemic-Type Aftershock Models

[10] Several authors have proposed different forms of point process models for the space-time clustering seismicity rate [*Ogata, 1998; also see Ogata, 1988, 1992; Kagan, 1991; Musmeci and Vere-Jones, 1992; Rathbun, 1993; Console and Murru, 2001; Console et al., 2003*]. These models are represented in terms of a conditional intensity function for the seismicity rate in time, space and magnitude (see *Daley and Vere-Jones [2003, chapter 7]* for mathematical details on the conditional intensity function). That is, at a particular time  $t$ , a location  $(x, y)$  and a magnitude  $M$ , it is formally defined by

$$\lambda(t, x, y, M | \mathcal{H}_t) = \frac{\Pr\{N(dt dx dy dM) = 1\}}{dt dx dy dM}, \quad (1)$$

where  $\Pr\{N(dt dx dy dM) = 1 | \mathcal{H}_t\}$  represents the probability of an event occurring in the infinitesimal volume  $dt dx dy dM$ , given the occurrence history  $\mathcal{H}_t$  up to time  $t$ . The mathematical term "conditional intensity means" "the occurrence rate of events conditional upon the observational history of previous events," hereafter referred to as the seismicity rate. The seismicity rate function of these models can be written in the common form of

$$\lambda(t, x, y, M | \mathcal{H}_t) = J(M) \left[ \mu(x, y) + \sum_{i: t_i < t} \xi(t - t_i, x - x_i, y - y_i; M_i) \right], \quad (2)$$

where the background seismicity rate  $\mu(x, y)$  is a function of space, but not of time. The contribution to the seismicity rate of an earthquake with magnitude  $M$ ,  $\xi(t, x, y; M)$ , has been assigned several forms by different authors. *Musmeci and Vere-Jones [1992]* use two diffusion-type response functions. In most other recent studies,  $\xi(t, x, y; M)$  takes, or can be represented by, a separable form,

$$\xi(t, x, y; M) = \kappa(M)g(t)f(x, y; M), \quad (3)$$

where  $\kappa(M)$  can be regarded as the expected number of events triggered by an event of magnitude  $M$ , and the function  $g$  and  $f$  are normalized, such that  $\int g(t) dt = 1$  and  $\iint f(x, y; M) dx dy = 1$ , representing the probability density function (PDF) of the occurrence time and location of a

direct offspring event, respectively. *Rathbun* [1993], *Ogata* [1998], and *Console et al.* [2003] took the form

$$\kappa(M) = Ae^{\alpha(M-M_C)} \quad M \geq M_C \quad (4)$$

$$g(t) = \frac{p-1}{c} \left(1 + \frac{t}{c}\right)^{-p}, \quad t > 0, \quad (5)$$

which is the PDF form of the modified Omori law (*Utsu* [1969] and *Omori* [1894] for the  $p = 1$  case). For the spatial PDF,  $f(x, y; M)$ , the following different functions have been used:

[11] Model 1 [*Rathbun*, 1993; *Console et al.*, 2003]

$$f(x, y; M) = \frac{1}{2\pi D^2} \exp\left[-\frac{x^2 + y^2}{2D^2}\right]; \quad (6)$$

model 2 [*Ogata*, 1998; *Zhuang et al.*, 2002]

$$f(x, y; M) = \frac{1}{2\pi D^2 e^{\alpha(M-M_C)}} \exp\left[-\frac{x^2 + y^2}{2D^2 e^{\alpha(M-M_C)}}\right], \quad (7)$$

where the parameter  $\alpha$  is the same one as in (4); model 3 [*Ogata*, 1998; *Console et al.*, 2003]

$$f(x, y; M) = \frac{q-1}{\pi D^2} \left(1 + \frac{x^2 + y^2}{D^2}\right)^{-q}; \quad (8)$$

model 4 [*Ogata*, 1998; *Zhuang et al.*, 2002, 2004]

$$f(x, y; M) = \frac{q-1}{\pi D^2 e^{\alpha(M-M_C)}} \left(1 + \frac{x^2 + y^2}{D^2 e^{\alpha(M-M_C)}}\right)^{-q}; \quad (9)$$

and in this paper, we also consider model 5 [*Ogata and Zhuang*, 2005]

$$f(x, y; M) = \frac{q-1}{\pi D^2 e^{\gamma(M-M_C)}} \left(1 + \frac{x^2 + y^2}{D^2 e^{\gamma(M-M_C)}}\right)^{-q}, \quad (10)$$

where  $\gamma$  is an independent parameter from  $\alpha$ .

[12] Central questions regarding the optimal choice among (6)–(10) are the following: (1) Do aftershocks decay in a short range (near-field, light tail) or a long range (far-field, heavy tail)? (2) Is the aftershock region scaled with the magnitude or the main shock? (3) If so, is its scale law the same as for the expected number of events? *Ogata* [1998], *Console et al.* [2003], and *Zhuang et al.* [2004] all showed that the aftershocks decay in a long range in different studies. In (7) and (9), the spatial scaling factor has the same exponent as the expected number of offspring events in (4). This is consistent with the conclusion of *Yamanaka and Shimazaki* [1990, equation [10]]. However, *Zhuang et al.* [2004] and *Ogata and Zhuang* [2005] found that the region of offspring locations can be scaled as an exponential law, but not the same exponential law as for the number of offspring. We therefore adopt the new model given in (10).

[13] The PDF for the distribution of the magnitude is

$$J(M) = \beta \exp[-\beta(M - M_C)], \quad M \geq M_C, \quad (11)$$

where the parameter  $\beta$  is linked to the Gutenberg-Richter's  $b$  value by

$$\beta = b \log 10. \quad (12)$$

[14] Since the distribution of the magnitude is independent of all other components and can be separated from the full joint likelihood of magnitudes, occurrences times and spatial locations, (2) can be separated by the following space-time seismicity rate function

$$\lambda(t, x, y | \mathcal{H}_t) = \mu(x, y) + \sum_{i: t_i < t} \kappa(M_i) g(t - t_i) f(x - x_i, Y - y_i; M_i). \quad (13)$$

### 2.3. Maximum Likelihood Estimates and Model Selection

[15] Given a set of observed earthquake data  $\{(t_i, x_i, y_i, M_i) : i = 1, 2, \dots, N\}$ , if the background rate  $\mu(x, y) = \nu u(x, y)$  where  $u(x, y)$  is known, the parameters in (13) can be estimated by maximizing the log likelihood [cf. *Daley and Vere-Jones*, 2003, chapter 7]

$$\begin{aligned} \log L(\boldsymbol{\theta}) = & \sum_{j: (t_j, x_j, y_j) \in [T_1, T_2] \times S} \log \lambda(t_j, x_j, y_j | \mathcal{H}_{t_j}) \\ & - \int \int_S \int_{T_1}^{T_2} \lambda(t, x, y | \mathcal{H}_t) dt dx dy, \end{aligned} \quad (14)$$

where  $\boldsymbol{\theta} = (\nu, A, \alpha, c, p, D)$  for models 1 and 2,  $\boldsymbol{\theta} = (\nu, A, \alpha, c, p, D, q)$  for models 3 and 4, and  $\boldsymbol{\theta} = (\nu, A, \alpha, c, p, D, q, \gamma)$  for model 5, and  $j$  runs over all the events in the study region  $S$  and time period  $[T_1, T_2]$ . It has been proved that the maximum likelihood estimates of these point-process models generally converge to their true values when the sample size (the number of events in the process) is large enough [*Ogata*, 1978; *Rathbun*, 1996].

[16] Because the events occurring outside of the study region, or before the study time period, may also trigger seismicity inside the study region and time period, particularly the large ones, we include these events in the observation history  $\mathcal{H}_t$  and call them complementary events. Events inside the study space-time zone, conversely, are called target events. Thus the complementary events only contribute to the seismicity rate function but are not included in the summation in the right-hand side of (14); that is, the subscript  $i$  runs over all the events in the catalogue in (2), while  $j$  in (14) runs over only the target events in the space-time zone  $[T_1, T_2] \times S$  of interest. As *Zhuang et al.* [2002] noted, information on the complementary large earthquakes should be included in the history if their contribution is substantial to the seismicity rate of the target events.

[17] The goodness-of-fit comparison between the above five models can be carried out using the Akaike information criterion (AIC) [see *Akaike*, 1974]. The statistic

$$AIC = -2 \max_{\boldsymbol{\theta}} \log L(\boldsymbol{\theta}) + 2k_p \quad (15)$$

is computed for each of the models fitted to the data, where  $k_p$  is the total number of fitted parameters. The model with the lowest AIC value is then taken as providing a better choice for future prediction purposes. Furthermore, AIC can be used as a rough guide for testing a model with  $k + d$  parameters against a null model with just  $k$  parameters. We take a difference of 2 in AIC values as a rough estimate of a significance level of 5%. If standard likelihood ratio asymptotics are applied, such a difference corresponds to a significance level of 4.6% when  $d = 1$ , 5.0% when  $d = 2$ , 4.6% when  $d = 3$ , and 3.5% when  $d = 5$  [see *Sakamoto and Akaike, 1978; Parzen et al., 1998*].

#### 2.4. Thinning Method and Stochastic Declustering

[18] The technical key point of the stochastic declustering method is the thinning operation to a point process (i.e., random deletion of points [cf. *Lewis and Shedler, 1979; Ogata, 1981; Daley and Vere-Jones, 2003*]). Observe (13), the relative contribution of a previous  $i$ th event to the total seismicity rate at the occurrence time and location of the  $j$ th event,  $(t_j, x_j, y_j)$ , is

$$\rho_{ij} = \begin{cases} \zeta_i(t_j, x_j, y_j) / \lambda(t_j, x_j, y_j | \mathcal{H}_{t_j}), & \text{when } j > i, \\ 0, & \text{otherwise,} \end{cases} \quad (16)$$

where

$$\zeta_i(t, x, y) = \kappa(M_i) g(t - t_i) f(x - x_i, y - y_i; M_i) \quad (17)$$

represents the rate triggered by the  $i$ th event. That is to say, given  $i$  fixed, for each  $j = i, i + 1, \dots, N$ , if we select the  $j$ th event with probability  $\rho_{ij}$ , we can realize a subprocess that consists of the direct offspring of the  $i$ th event. In this way,  $\rho_{ij}$  can be naturally regarded as the probability that the  $j$ th event is a direct offspring of the  $i$ th event. Furthermore, the probability of the event  $j$  being a background event is

$$\varphi_j = \frac{\mu(x_j, y_j)}{\lambda(t_j, x_j, y_j | \mathcal{H}_{t_j})}, \quad (18)$$

and the probability that the  $j$ th event is triggered by previous events is given by

$$\rho_j = 1 - \varphi_j = \sum_i \rho_{ij}. \quad (19)$$

In other words, if we select each event  $j$  with probabilities  $\varphi_j$ , we can then form a new processes, the background subprocess with a rate function  $\mu(x, y)$ , and its complement, the clustering subprocess.

[19] A stochastic declustered catalogue produced from the above procedures is not unique, because it depends on the random numbers used in the selection of events to form the background seismicity. This method gives the probabilities of how likely each event is to be a background event or to be triggered by other events, but does not make a fixed judgment on whether an event is an aftershock or not. This should be considered as an advantage of the method, since it allows uncertainty about the declustering to be quantified. By repeating random selection, we can easily produce many copies of the declustered catalogue, from which we can

evaluate the uncertainty or significance of a particular feature associated with the declustered catalogue.

#### 2.5. Variable Kernel Estimates of Seismicity Rates

[20] The total spatial seismicity rate can be estimated by using variable kernel estimates

$$\hat{m}(x, y) = \frac{1}{T} \sum_j Z_{h_j}(x - x_j, y - y_j), \quad (20)$$

where  $T$  is the length of the time period of the process, subscript  $j$  runs over all the event in the process and  $Z$  is the Gaussian density function [*Zhuang et al., 2002*]. The variable bandwidth  $h_j$  (the standard deviation of the Gaussian density) is determined by

$$h_j = \max\{\epsilon, \inf\{r : N[B(x_i, y_i; r)] > n_p\}\}, \quad (21)$$

where  $\epsilon$  is the allowed minimum bandwidth,  $B(x, y; r)$  is the disk of radius  $r$  centered at  $(x, y)$ , and  $n_p$  is a positive integer; that is,  $h_j$  is the distance to its  $n_p$ th closest neighbor.

[21] Once the thinning probabilities  $\varphi_j$  are obtained, we can estimate the spatial background seismicity rate by using weighted variable kernel estimates [*Zhuang et al., 2002*],

$$\hat{\mu}(x, y) = \frac{1}{T} \sum_j \varphi_j Z_{h_j}(x - x_j, y - y_j), \quad (22)$$

where  $T$ ,  $Z$  and  $h_j$  are defined as in (20). Equation (22) is equivalent to the average of kernel estimates for the spatial seismicity rate in many realizations of the background catalogues produced by using the thinning method (stochastic declustering), i.e.,

$$\hat{\mu}(x, y) = \mathbf{E} \left[ \frac{1}{T} \sum_j X_j Z_{h_j}(x - x_j, y - y_j) \right], \quad (23)$$

where the random variables,  $X_j, j = 1, \dots, N$ , independently takes values 1 or 0 with probability  $\varphi_j$  and  $1 - \varphi_j$ , respectively, and  $\mathbf{E}[\ ]$  represents the average over all the combinatorial realizations of  $\{X_j; j = 1, 2, \dots, N\}$ .

[22] By simply taking the difference between the total seismicity rate and the background seismicity rate, we can get the estimate of the clustering rate function; that is, the estimate of the clustering rate is

$$\hat{C}(x, y) = \hat{m}(x, y) - \hat{\mu}(x, y) = \frac{1}{T} \sum_j (1 - \varphi_j) Z_{h_j}(x - x_j, y - y_j). \quad (24)$$

To show the degree of clustering, we also define the clustering ratio function as the ratio of the clustering seismicity rate to the total seismicity rate,

$$\Omega(x, y) = \frac{\hat{C}(x, y)}{\hat{m}(x, y)}. \quad (25)$$

If  $m(x, y)$  is too small, the clustering ratio is then of high uncertainty. In general, the reliability of the clustering ratio

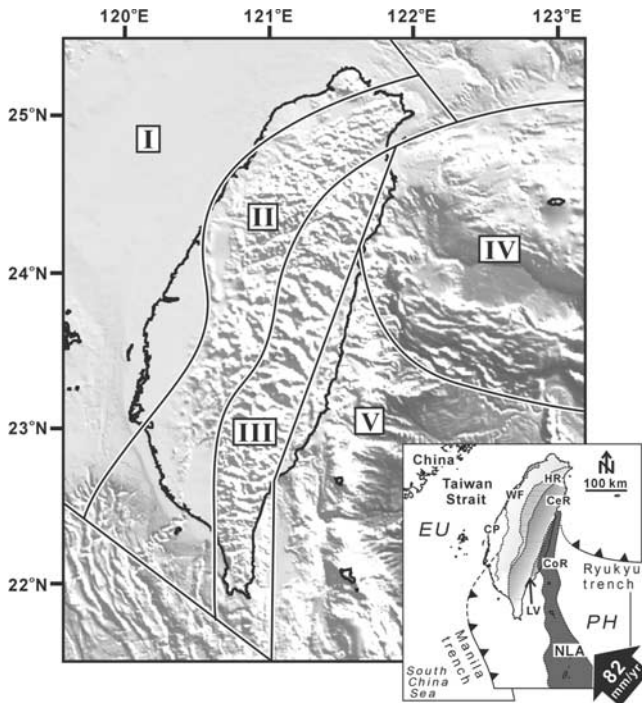


**Figure 1.** Seismotectonic zones of the Taiwan area. CP, Coastal Plain; CeR, Central Range; CoR, Coastal Range; EU, Eurasian plate; HR, Hsüehshan Range; LV, Longitudinal Valley; NLA, northern Luzon volcanic arc; PH, Philippine plate; WF, Western Foothills.

depends on the value of the total seismicity rate; that is, the higher the total seismicity rate, the more reliable the clustering ratio.

[23] The problem regarding the optimal selection of  $n_p$  for the variable bandwidth for the statistics in (20), (22), and (24) can be solved in the following way. Remembering that the integral of the clustering term on the right side of (13) with respect to time,

$$I(x, y) = \frac{1}{T} \int_0^T \sum_{i:t_i < t} \kappa(M_i) g(t - t_i) f(x - x_i, y - y_i; M_i) dt, \quad (26)$$

also provides an image of the clustering seismicity rate in space, but not smoothed, we can, in principle, select a suitable  $n_p$  by minimizing the discrepancy between the low-frequency (smoothed) component of  $I(x, y)$  in (26) and  $\hat{C}(x, y)$  in (24). In practice, however, because the estimates are rather insensitive to the choice of  $n_p$ , a rough estimate is generally sufficient.

## 2.6. Algorithm for Simultaneously Estimating the Background Seismicity Rate and Model Parameters

[24] Background seismicity and the parameters can be determined in the clustering structures simultaneously using an iterative approach [Zhuang *et al.*, 2002, 2004]. First, we assume some initial background seismicity rate, using the maximum likelihood procedure to obtain the parameters in the branching structure. We then calculate the background probabilities  $\{\varphi_j; j = 1, 2, \dots, N\}$  for all of the events using

(18). Substituting these  $\varphi_j$  into (22), we get a better estimate of the background seismicity rate, and use this newly estimated background seismicity rate to replace the initial background rate. We repeat these steps many times until the results converge.

[25] This algorithm converges quickly, usually in 5 to  $\sim 20$  steps. Zhuang *et al.* [2002] showed that for the central New Zealand catalog of shallow earthquakes, the algorithm converged within 10 steps.

## 3. Tectonic Background and Data Selection

### 3.1. Tectonic Background

[26] The island of Taiwan is located at the junction between two subduction systems. To the east, the Philippine plate (PH) subducts along the Ryukyu subduction system, northward beneath the Eurasian plate (EU), while to the south, the Philippine plate overrides the crust of the South China Sea at the Manila trench (Figure 1). According to GPS observations, the convergent rate between the northern Luzon volcanic arc (NLA in the inset diagram of Figure 1), which is located on the Philippine plate, and the southeast Eurasian continental margin is about 8.2 cm/yr with an azimuth of  $310^\circ$  [Yu *et al.*, 1997].

[27] The general structural trends of the Taiwan mountain belt show an elongated S shape. As a result of regional compression, the island of Taiwan consists of several provinces [Ho, 1986] with a main structural grain that tends approximately along the NNE direction (see Figure 1 inset), namely, from west to east, the Coastal Plain, the Western Foothills, the Hsüehshan Range, the Central Range, and the Coastal Range. The Coastal Plain, Western Foothills and Hsüehshan Range in western Taiwan are composed of thick sequences of Cenozoic shallow marine siliciclastics. The Western Foothills and Hsüehshan Range are deformed by a combination of folds and thrust faults, which tend mainly northeast or northward and dip toward the east or southeast [Suppe, 1980; Ho, 1986]. The basement of the Central Range is composed of the pre-Tertiary complex affected by Neogene greenschist facies and higher grades of polyphase Mesozoic-Cenozoic metamorphism. East of the Central Range, the Coastal Range is mainly composed of Neogene andesitic volcanic units and associated flyschoid and turbidite sediments, which belong to the Philippine plate [Ho, 1986] and represent a section of the Luzon arc that is being accreted onto the Eurasian continent (Figure 1). It is worthwhile to mention that the suture zone between the eastern Central Range and the Coastal Range, the Longitudinal Valley, is also one of the most active deformation zones in Taiwan [Tsai, 1986; Yu *et al.*, 1997].

[28] From the distribution of seismicity, Tsai *et al.* [1997] divided the boundary between the Eurasian and Philippine plates in the Taiwan area into three segments. Generally following their suggestion, our division differs in that we also consider the regional tectonic background. In this study, the Taiwan area has been divided into five seismotectonic zones, namely, zone I, the Taiwan Strait and Coastal Plain; zone II, the Western Foothills and Hsüehshan Range; zone III, the Central Range; zone IV, the Ryukyu subduction system; and zone V, the Coastal Range and the Philippine plate (Figure 1).

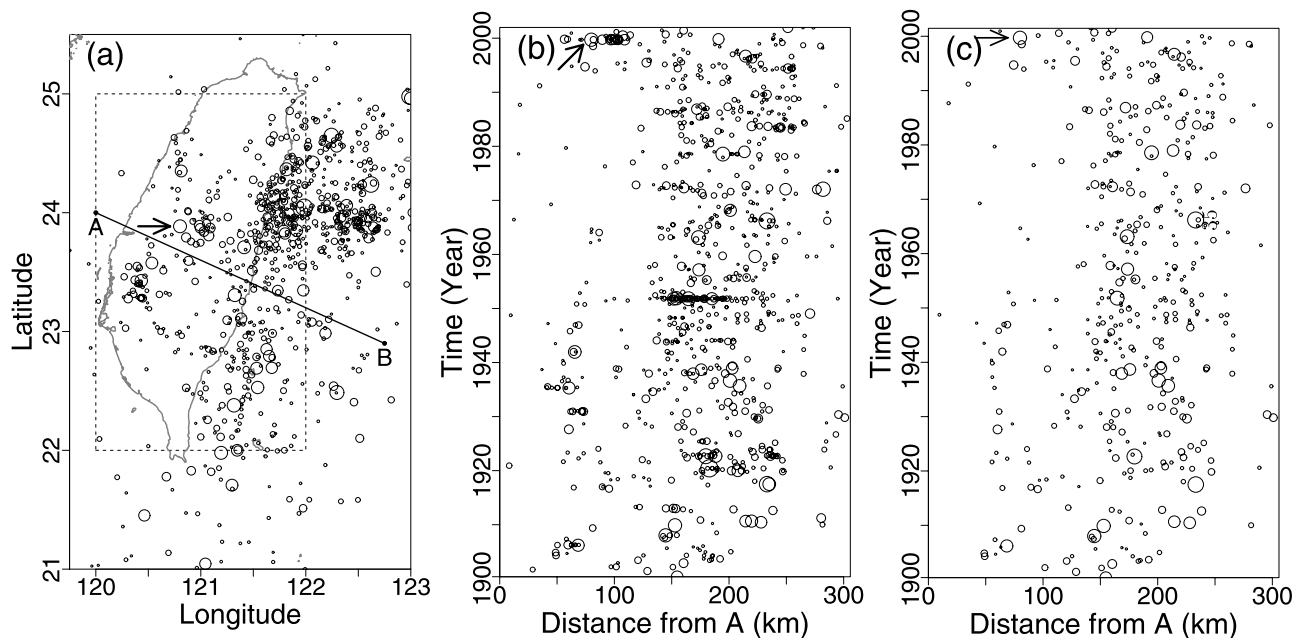


**Figure 2.** (a) Epicentral map of the earthquakes. The dashed rectangular box represents the study region for the target events (see section 2.3). (b) Space-time plot of earthquakes with epicenters projected on the line segment AB. Horizontal axis represents the projected distance from A, and vertical axis represents the occurrence times. (c) Same space-time plot for a realization of the background events. The arrows indicate the Chi-Chi earthquake.

### 3.2. Data Selection

[29] The history of the monitoring network in Taiwan can be mainly divided into several periods [Wang, 1998]:

[30] 1. From 1897 onward, three-component low-gain displacement seismometers were installed at 17 stations in the Taiwan region by Japanese seismologists, used during the period 1897–1935. Because of the nonsynchronous timing system, remarkable errors for arrival times result in high errors in earthquake locations. Some acceleration seismometers and strong motion seismometers were put into use in 1951, and in 1963, a World Standard Network station was constructed in Anpu, equipped with two high-gain electric record seismometers, one of long period and one of short period.

[31] 2. The Taiwan Telemetered Seismographic Network (TTSN) of 24 stations was constructed from 1972, each station equipped with a three-component high-gain and analog velocity seismometer.

[32] 3. In 1991, the Taiwan Seismic Network (TSN) was upgraded from the old Central Weather Bureau (CWB) seismic network, consisting of 72 stations, each equipped with three-component digital velocity seismometers.

[33] A complete and homogeneous earthquake catalogue is important for the ETAS fitting. Taking the above discussion into consideration, we take the target events of  $M \geq 5.3$  and depths  $\leq 55$  km in the period from 1 January 1941 (14,975 days from 1 January 1900) to 31 December 2001 and in the region ( $120\text{--}122^\circ\text{E}$ ,  $22\text{--}25^\circ\text{N}$ ; see Figure 2a) for estimating the parameters, the events with a magnitude no less than 5.3 outside the target region and period are used as the complementary events; that is, they do not directly contribute to the likelihood function, but influence the seismicity rate function (see

section 2.3). The starting time 1 January 1941 is chosen for the reason that, from this time point onward, the observation conditions had been stabilized after the 17 stations were constructed.

### 4. Parameters and Spatial Intensities of the Background and Clustering Seismicity

[34] According to the principle in section 2.5, we use  $n_p = 3$  and  $\epsilon = 0.05$  deg in the variable kernel estimates of the background rate, where  $1$  deg  $\approx 111.1$  km, meaning  $1/360$  of the great arc of the Earth's surface, approximated by a sphere. The estimated parameters for the branching structures of the five models are listed in Table 1. Among these models, model 5 is chosen as the best fit to the Taiwan data, which again confirms the following conclusions on the spatial distribution of directly triggered events: (1) the triggered events decay in a long range decay rather than a short-range decay; (2) the aftershock region is scaled by an exponential law of the magnitude of the ancestor event; and (3) the above spatial scaling law is not the same as the exponential law for the expected number of events.

[35] The AIC values indicate that models 1 and 3 fit the data better than models 2 and 4, respectively. This does not imply that the aftershock region shown be scaled by a constant. The reason why this holds is that the difference between the exponents  $\alpha$  and  $\gamma$  is too large. That is to say, if the two exponents do not differ much from one another, models 2 and 4 would provide a better fit than models 1 and 3, respectively. Simply assuming that the two exponential laws take the same exponents may lead to the wrong conclusion that scaling the aftershock region is unnecessary. Indeed, the minimum AIC is obtained by model 5, which

**Table 1.** Results From Fitting Models 1–5 to the Selected Taiwan Data<sup>a</sup>

Model	$A$	$\alpha$	$c$	$p$	$D^2$	$q$	$\gamma$	$\log L$	AIC
1	0.205	1.684	$4.315 \times 10^{-3}$	1.132	$2.179 \times 10^{-2}$	NA	NA	-1405.5	2823.0
2	0.182	1.694	$6.692 \times 10^{-3}$	1.150	$2.868 \times 10^{-3}$	NA	NA	-1411.1	2834.2
3	0.204	1.654	$4.761 \times 10^{-3}$	1.139	$1.855 \times 10^{-2}$	1.978	NA	-1393.6	2801.1
4	0.234	1.504	$5.089 \times 10^{-3}$	1.141	$3.194 \times 10^{-3}$	1.839	NA	-1397.6	2809.2
5	0.183	1.766	$5.094 \times 10^{-3}$	1.140	$8.314 \times 10^{-3}$	1.945	0.689	-1390.6	2797.2 <sup>b</sup>

<sup>a</sup>NA, not applicable.

<sup>b</sup>the smallest AIC value.

supports the spatial scaling by the magnitude of the direct ancestor.

[36] In evaluating the spatial variations of the total seismicity rate, the background seismicity rate, clustering seismicity rate, and clustering ratio, we extend the calculation over a larger region (21.5–25.2°N, 120–123°E) than the study region (22–25°N, 120–122°E), with the parameters obtained from fitting model 5 to the data of events only falling within the study space-time zone. The distribu-

tions of the above variables, as shown in Figures 3, indicate the following:

[37] 1. The total seismicity rate's, as shown by the logarithm scale in Figure 3a, biggest contribution comes from the convergence part on the plate boundaries. The most active region is on the northern part of the convergence line, where the Philippine plate is subducting underneath the Eurasian plate. The total seismicity rate decreases with distance from the convergence lines, although is

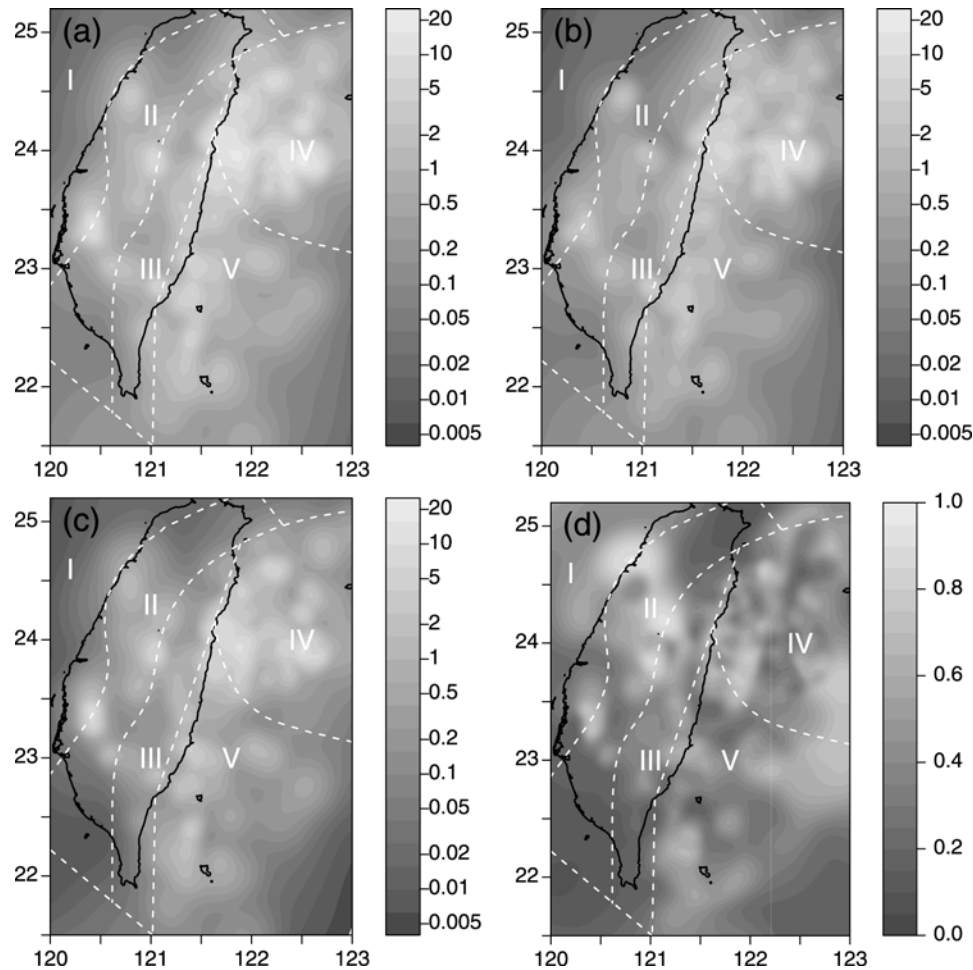


**Figure 3.** Estimated seismicity rates: (a) total seismicity rate  $\hat{m}(x, y)$ , (b) background seismicity rate  $\hat{\mu}(x, y)$ , (c) clustering seismicity rate  $\hat{C}(x, y)$ , and (d) clustering ratio  $\Omega(x, y)$ . See equations (20), (22), (24), and (25) for the definitions, respectively. The unit of the images for the rates in Figures 3a–3c is events/(degree<sup>2</sup> year). The uncertainty of the values of the clustering ratio at each location in Figure 3d can be roughly evaluated through the values of the total seismicity rate in Figure 3a or through the density of events in Figure 2a (see section 2.5). See color version of this figure at back of this issue.

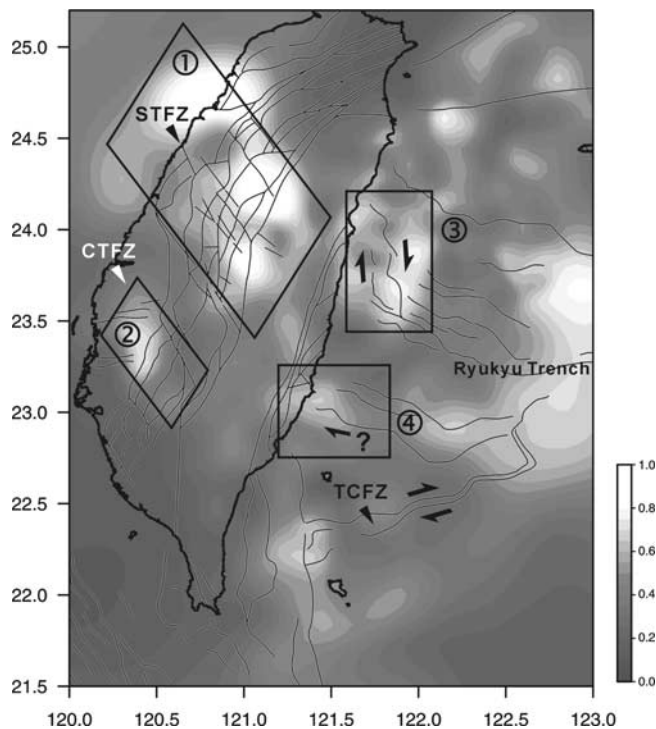


**Figure 4.** Distribution of seismic clustering ratio and structural interpretation of the Taiwan area. Surface faults are shown in solid lines as interpreted from multisources (data after *Mining Research and Service Organization* [1982], *Deffontaines et al.* [1994, 1997], *Lallemand and Liu* [1998], *Schmurle et al.* [1998], and *Kao et al.* [2000]). STFZ, Sanyi transfer fault zone; CTFZ, Chiayi transfer fault zone; TCFZ, Taitung Canyon Fault Zone. Details of the four areas with high clustering ratio (shown by white frames) are discussed in the text. See color version of this figure at back of this issue.

relatively low in the middle inland region, such as in the Hsüehshan Range. The western inland areas have several local maxima in the total seismicity rate, caused by several big earthquake sequences or swarms.

[38] 2. The background seismicity rate, estimated using (22) to remove the clustering components, does not vary as much as the total seismicity rate does. The high values of the background seismicity rate are distributed along the convergence line between the collision of Philippine and Eurasian plates and off the east coast of the island of Taiwan. Overall the high background seismicity rate shows a pattern of belts, which are distributed parallel to the tectonic structure lines.

[39] 3. The clustering seismicity rate contains most of the irregular components of the total seismicity, since the background part is removed. The absolute values of highest clustering seismicity along the Ryukyu Trench are much higher than in other regions.

[40] 4. The clustering ratio appears largely differentiated from the above variations. The rates of both background and clustering seismicity are both high along the Ryukyu Trench, although the clustering ratio changes dramatically. The clustering ratio is high in the western part but very low in the eastern part. In the northwestern inland areas, the

background seismicity rate is much lower than in the northeastern subregion, although a higher clustering ratio implies that it is not so easy to have an earthquake inside, but that, once a large earthquake occurs, it is followed by a large number of aftershocks with very high probability. Furthermore, the asperities of the fault are expected to be in the region of the low clustering ratio but next to the high background and high clustering ratio [cf. *Ogata*, 2004]. These features should be considered for the evaluation of the losses caused by future earthquakes. Seismicity in the southwest inland region shows less clustering, but still shows a similar feature. The difference between this and the northwest inland region may be caused by the geological properties of regional crustal materials, as shown in Figure 1.

## 5. Interpretation of the High Clustering Ratio Regions by the Tectonic Structures

[41] As mentioned in sections 1–4, the distribution of seismicity of the Taiwan area can be explained largely by the convergent tectonic framework between the Eurasian and Philippine plates. Nevertheless, the spatial variation of the clustering ratio reveals a more complex pattern, different from the seismic rates. For example, around the eastern distal part of the Ryukyu Trench, both background and clustering seismicity are of high rate, while the clustering ratio of this area remains very low (Figures 3 and 4). The significance of our calculated clustering ratio will be discussed in this section.

[42] At first approximation, four areas of high clustering ratio can be recognized around the Taiwan island, namely (1) the central western Taiwan area, (2) the southwestern Taiwan area, (3) the eastern Taiwan area, and (4) the southeastern Taiwan area (Figure 4). Comparison of the pattern of the clustering ratio with local tectonic background shows that the first two areas (areas 1 and 2) seem to have close geometrical correlations with so-called oblique structures within the Taiwan Foothills proposed by previous studies [e.g., *Ho*, 1979, 1986; *Pelletier and Stephan*, 1986; *Deffontaines et al.*, 1997]. In western Taiwan, the Foothills display active asymmetric folds and low-angle thrust faults, fold axes tend mainly  $N20^{\circ}E$  and have steep to overturned western flanks commonly cut by WNW vergent thrust faults. However, on the basis of subsurface data [e.g., *Sun*, 1963, 1964], satellite images (SPOT), digital elevation models (data after Taiwan Forestry Bureau), side-looking airborne radar (SLAR) images, aerial photographs and local field work, *Deffontaines et al.* [1994, 1997] identify a series of structures tending mainly  $N140^{\circ}E$  oblique to the fold-and-thrust belt in the Western Foothills. These  $N140^{\circ}E$  tending structures are believed to correspond to transfer faults, that is to strike-slip faults parallel to the thrust transport direction that separates two parts of a given thrust sheet, each of which may have different displacements and deformations [*McClay*, 1992]. Among these transfer faults there are two important zones which can be defined: the Sanyi and the Chiayi transfer fault zones. These two transfer fault zones also display a high seismic activity, and the distribution of earthquakes and the related focal mechanisms confirm the left-lateral movement along  $N140^{\circ}E$  directions. The results of our study show that in western

Taiwan the clustering ratio around the Sanyi and the Chiayi transfer fault zones is much higher than that of other areas (Figure 4). This phenomenon provides us with important information that can be used to explain the effect of seismic clustering.

[43] For further examination of the relationship between the seismic clustering ratio and the regional tectonic framework, we pay close attention to the area of eastern Taiwan (area 3). This area connects the Ryukyu Trench and the northern tip of the Longitudinal Valley (see area III in Figure 1) and also displays a high clustering ratio. Although the structural pattern in this transitional area is very complex, the transcurrent faults are the most obvious structures [Lallemand and Liu, 1998]. As a result of stress partitioning, the westernmost segment of the Ryukyu accretionary wedge has been dragged toward the island of Taiwan, forming this series of major right-lateral faults [Dominguez et al., 1998; Lallemand et al., 1999]. The observation from this area further leads us to believe that the clustering ratio has a very close relationship with the strike-slip structure.

[44] The last area (area 4) with a high clustering ratio around the Taiwan island is in the southeastern offshore Taiwan. The tectonic background of this area is still not clear. This area runs eastward along the axis of a submarine canyon, which merges with the Taitung Canyon Fault Zone (TCFZ) near the Ryukyu trench (Figure 4). On the basis of seismic observations, morphological features, and magnetic anomalies, Kao et al. [2000] identified that the TCFZ is a large-scale right-lateral strike-slip fault. Moreover, they suggested that this fault system probably has repeatedly changed its position in response to the propagation of Taiwan's arc-continental collision. In other words, the current TCFZ must be a recently developed structure and will be abandoned once the transition migrates farther to the southwest. Their proposition suggests that there may be some strike-slip fault traces at the north of the TCFZ and our results provide a possible candidate for this model. The clustering ratio along the TCFZ is also high and confirms our previous observations.

## 6. Stochastic Declustering Output and Background Seismicity

[45] Figure 3 gives the spatial variation of the background rates, based on the model formulation that it is stationary in time but nonhomogeneous in location. In fact, background seismicity often departs from stationarity, which may be influenced by changes of regional tectonic stress field. To understand how the background seismicity changes, we can use the thinning procedure mentioned in section 2.3 to realize different stochastic versions of declustered catalogues and to detect the existence of changes of occurrence rates in these catalogues. Figure 2c shows the epicenter maps and space-time plot of an example version of the background catalogues. It seems that there is a quiescent period in the background seismicity around the source of the 21 September 1999 Chi-Chi earthquake ( $M_S$  7.9) from the mid-1950s to the mid 1990s, while the background occurrence rate in the eastern areas seems to be stationary. Similar patterns can be also found in the space-time plot for all of the events (Figure 2b), although the stationarity of the background catalogue cannot be easily identified in eastern

parts (a projection distance of more than 130 km from location A).

[46] To discuss how the background seismicity changes with time in section 7, we can use the thinning procedure mentioned in section 2.3 to realize different stochastic versions of declustered catalogues and then detect the existence of changes of occurrence rate in them. However, a more direct way is to calculate the cumulative background seismicity,

$$S(t) = \sum_{t_i < t} \varphi_i, \quad (27)$$

where  $\varphi_i$  is the background probability defined in (18) and  $i$  runs over the events in some specified region. Similarly, the cumulative clustering seismicity can be evaluated by

$$C(t) = \sum_{t_i < t} (1 - \varphi_i). \quad (28)$$

If the model fits the seismicity well or the background occurrence rate is a constant function of time, the function  $S(t)$  defined by (27) increases approximately in a constant rate with time  $t$ . If the slope of  $S(t)$  decreases, we call it quiescence in background seismicity, or simply background quiescence; otherwise, if the slope of  $S(t)$  increases, we call it an activation in the background seismicity, or simply background activation.

## 7. An Interpretation of the Seismicity Patterns Preceding the Chi-Chi Earthquake

[47] It may be worthwhile to provide here a speculation of aseismic slips that may have taken place somewhere in or around the fault of the 1999 Chi-Chi earthquake, which could change the Coulomb stress failures. The Coulomb stress change is give by

$$\Delta\text{CFS} = \Delta(\text{shear stress}) - \mu_f \times \Delta(\text{normal stress}), \quad (29)$$

where  $\mu_f$  is the apparent friction coefficient. Hereafter, we set  $\mu_f = 0.4$ , and the  $\Delta\text{CFS}$  in a elastic half-space [Okada, 1992] is calculated by assuming a shear modulus  $3.2 \times 10^{11}$  dyn  $\text{cm}^{-2}$  and a Poisson ratio of 0.25. Positive values of  $\Delta\text{CFS}$  promote failure and negative ones inhibit failure (the stress shadow). Then, this would result in quiescence in background activity in the stress shadow regions, while activity in other regions would remain.

[48] In order to make a quantitative scenario, owing to the  $\Delta\text{CFS}$ , we rely on the simple preliminary model of the Chi-Chi rupture adopted by Yoshioka [2001], which further provides detailed coseismic slip distribution on the fault plane by geodetic data inversion based on the GPS displacement data, taking into account the shape of the surface rupture and the centroid moment tensor solutions; that is, a fault size of 70 km  $\times$  50 km, a dip angle of  $31^\circ$  and strike of  $N9^\circ\text{E}$ , leading to the average coseismic slip and direction of 5.1m and  $N55^\circ\text{W}$  (the rake angle  $64^\circ$ ), respectively. We hereby assume an aseismic slip zone on the deeper half of the fault plane of the Chi-Chi rupture source. Explicitly allowing for the calculation, we assume the same fault

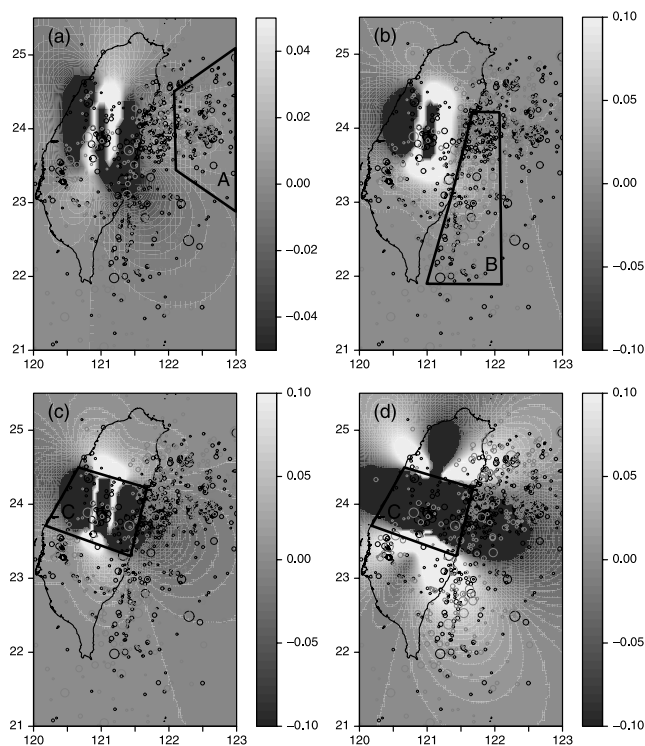


**Figure 5.** Distribution of  $\Delta\text{CFS}$  in the three typical seismic regions in Taiwan and its vicinity, caused by the assumed aseismic slip on the deeper part of the Chi-Chi earthquake fault (see text for the detail): (a) far offshore to the northeast of Taiwan Island (region A) at the depth of 30 km with receiver fault angles of (strike, dip, rake) =  $(270^\circ, 30^\circ, 90^\circ)$ ; (b) eastern offshore region (region B) to the LV (Longitudinal Valley) at the depth of 25 km with receiver fault angles  $(10^\circ, 15^\circ, 80^\circ)$ ; (c) central inland region (region C) at the depth of 15 km with receiver fault angles  $(10^\circ, 30^\circ, 60^\circ)$ ; (d) central inland region (region C) as in Figure 5c, but with receiver fault angles  $(135^\circ, 90^\circ, 0^\circ)$ . The unit of the  $\Delta\text{CFS}$  is given in bars. The depths are chosen at which most earthquakes occur inside the corresponding regions. See color version of this figure at back of this issue.

length and angles for the aseismic slip as those of the main rupture, but assume that the top of the slip zone is 12.5 km deep, the width of the slip zone is 25 km, with the slip size tentatively being given as 10% ( $\approx 50$  cm) of that estimated for the main rupture.

[49] Seismicity regions in and around Taiwan are classified roughly into three regions by taking into account local tectonic structures and the hypocenter distributions. The first region is in the far offshore region of the northern half of the island of Taiwan (region A), included in the region IV of Figure 1. The seismicity here is mostly interplate earthquakes beneath the Eurasian plate, where the Philippine plate is subducting northward along the Ryukyu Trench. Therefore we consider receiver fault angles of (strike, dip, rake) =  $(270^\circ, 30^\circ, 90^\circ)$ . The pattern of the  $\Delta\text{CFS}$  values in this region at a depth of 30 km are given in Figure 5a. These are small but positive in all depth ranges down to a depth of 50 km. The background seismicity in

this region, given in Figure 6b, shows slightly increasing activity after the 1940s, although this may be due to the improvement of detection rate of  $M5.5$  events or greater in such an offshore region from the land. At the very least, however, we see steady activity after the 1940s, continuing through to the present-day.

[50] The second region is in the eastern offshore region of the Longitudinal Valley (LV) (region B), included mostly in region V. The dominating earthquake mechanism here is oblique-reverse faulting with a small strike-slip component. The dip angles are high ( $50$ – $60^\circ$ ) in the proximity of LV but are low ( $10$ – $15^\circ$ ) offshore. Therefore we consider receiver fault angles of  $(10^\circ, 15^\circ, 80^\circ)$ . The pattern of the  $\Delta\text{CFS}$  values in this region at a depth of 25 km are given in Figure 5b. Another nonnegligible mechanism is the north to NNW right-lateral strike slips in the northern part of region B (see area 3, Figure 4) as stated in section 6. Thus we also

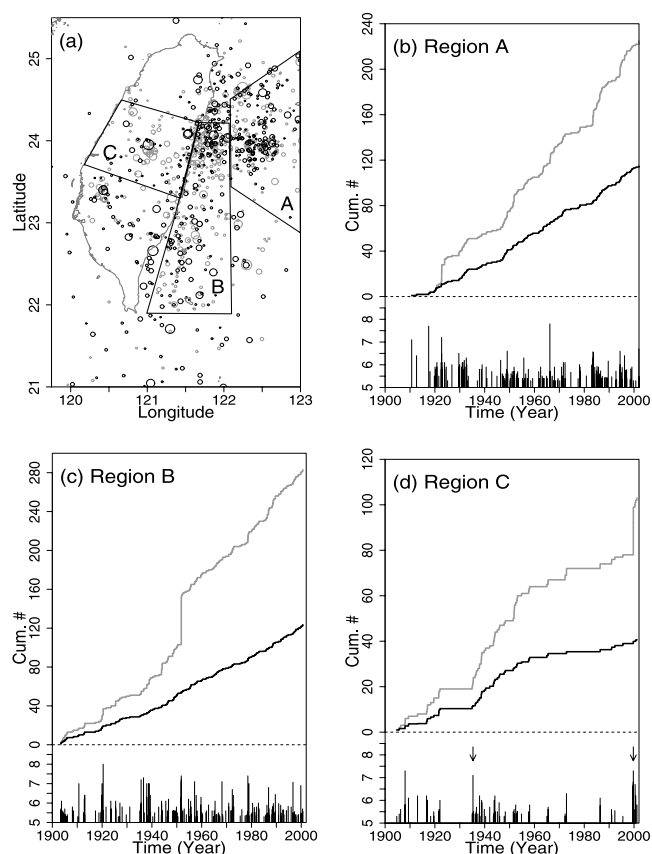


**Figure 6.** (a) Illustration of regions classified by tectonics and  $\Delta\text{CFS}$  pattern. Circles represent a stochastic separation of background events (black circles) and clustering events (gray circles). Different circle sizes represent the magnitude. Cumulative curves of the background events in regions A, B and C are plotted in Figures 6b, 6c, and 6d in black step functions, respectively. The corresponding cumulative curves of the total events are represented by gray step functions. The plot of magnitudes against times for each corresponding region is at the bottom of each panel. The arrows in Figure 6d indicate the Shin-Chu Taichung earthquake ( $120.81^\circ\text{E}, 24.35^\circ\text{N}$ ;  $M7.1$ ; 21 April 1935) and the Chi-Chi earthquake ( $120.80^\circ\text{E}, 23.89^\circ\text{N}$ ;  $M7.3$ ; 21 September 1999).

examined the receiver fault angles of (170°, 90°, 180°). The pattern of the  $\Delta CFS$  values in this region at a depth of 15 km is positive or neutral, except for those values in the southwestern part of region B, which are stable for ranges of shallow depth (0–30 km). The background seismicity in this region, given in Figure 6c, shows slightly increasing activity after the 1940s, and we see steady activity after the 1940s, as seen in the previous case.

[51] The third region is inland Taiwan, the western side of the Longitudinal Valley (LV) included in the regions II and III of Figure 1. Here we assume either a thrust-type mechanism similar to the Chi-Chi rupture (strike, dip, rake) equal to (10°, 30°, 60°) or a northwest left-lateral strike-slip faulting (135°, 90°, 0°) for the transfer faults as described in section 5. The respective  $\Delta CFS$  patterns at a depth of 15 km are provided in Figures 5c and 5d. The stress shadows of both cases cover the middle latitude area of inland Taiwan (region C), with the stress shadow being shown in proximity of the LV in the same region, due to a high dip angle (50–60°) of the oblique-reverse faulting, as described in the above case. The background seismicity in this region is given in Figure 6d and shows a quiet period from 1960–1990, followed by recovery of activity culminating with the Chi-Chi rupture. It can also be seen from the positive  $\Delta CFS$  around the hypocenter at a depth of 8–10 km that the assumed aseismic slip strongly encourages occurrence of the Chi-Chi rupture. Such positive  $\Delta CFS$  near the hypocenter does exist even if we change the parameters of the aseismic fault in a reasonable degree. Incidentally, we clearly see additional quiescence during a period of about 15 years prior to the 1935 Shin-Chu Taichung earthquake of  $M7.1$  (120.81°E, 24.35°N), for which we may assume a similar scenario.

## 8. Conclusion

[52] To analyze seismicity in the Taiwan region, we have applied the space-time ETAS model, and then applied the stochastic declustering method, which stochastically separates the whole seismicity during the last 100 years into background and clustering seismicity. Thus imaging of the separated quantities is performed in order to discuss implication of the regional features of seismicity in and around Taiwan.

[53] The zones of highest background seismicity rates correspond to the zones of high stress accumulation on the tectonic boundaries, such as the large transfer fault zones along the eastern part of Longitudinal Valley and the northern region of the Ryukyu trench, beneath which lies the boundary of the Eurasian plate and the subducting Philippine plate. On the other hand, the regions of highest clustering seismicity rate correspond to the aftershock area of strong earthquakes. The contrast of the above two seismicity rates is enhanced by taking the ratio of the clustering seismicity rate to the total seismicity rate (clustering ratio). Its geological interpretation has also been discussed in relation to the known major strike-slip faults in Taiwan. In particular, comparison of these data leads to the following remarks: (1) The central western and the southwestern inland areas have a high clustering ratio accompanied by large transfer fault zones, especially with regards the central western area. (2) The high clustering ratio

area at the eastern offshore area has a series of major right-lateral faults. (3) The high clustering ratio of the southeastern offshore area may be related to a strike-slip fault trace.

[54] The temporal features of the background seismicity in the central inland regions show a conspicuously quiet period lasting up to several decades, prior to recovery of the activity, culminating in the 1999 Chi-Chi earthquake, while other major seismic regions remain active stationarily. Assuming precursory slips in the deeper part of the Chi-Chi earthquake fault, we can explain these different seismicity patterns by changes in Coulomb failure stresses. From these we can see that only central western area of inland Taiwan becomes a stress shadow.

[55] **Acknowledgments.** This study was partially supported by A-91-N-FA07-7-4 from the Ministry of Education, Taiwan, and Grant-in-aid 1680334 for the Scientific Research from the Ministry of Education, Science, Sport and Culture, Japan. The first author is also supported by a postdoctoral program funded by the Japan Society for the Promotion of Science. Discussions with Chang Tsui-Yu, Ma Kuo-Fong, and Tsai Yi-Ben from the National Central University have also been useful in preparing this paper. The authors also thank Massimo Cocco, R. Console and an anonymous referee for their helpful comments and suggestions.

## References

- Akaike, H. (1974), A new look at the statistical model identification, *IEEE Trans. Automat. Control*, AC-19, 716–723.
- Console, R., and M. Murru (2001), A simple and testable model for earthquake clustering, *J. Geophys. Res.*, 106, 8699–8711.
- Console, R., M. Murru, and A. M. Lombardi (2003), Refining earthquake clustering models, *J. Geophys. Res.*, 108(B10), 2468, doi:10.1029/2002JB002130.
- Daley, D., and D. Vere-Jones (2003), *An Introduction to Theory of Point Processes*, Springer, New York.
- Davis, S. D., and C. Frohlich (1991), Single-linked cluster analysis, synthetic earthquake catalogs, and aftershock identification, *Geophys. J. Int.*, 104, 289–306.
- Deffontaines, B., J. C. Lee, J. Angelier, J. Carvalho, and J. P. Rudant (1994), New morphotectonic data in Taiwan: Analyses of digital elevation model, SPOT and radar images, and geodynamic implications, *J. Geophys. Res.*, 99(B10), 20,243–20,266.
- Deffontaines, B., O. Lacombe, J. Angelier, H. T. Chu, F. Mouthereau, C. T. Lee, J. Deramond, J. F. Lee, M. S. Yu, and P. M. Liew (1997), Quaternary transfer faulting in Taiwan Foothills: Evidence from a multi-source approach, *Tectonophysics*, 274, 61–82.
- Dominguez, S., S. Lallemand, J. Malavieille, and P. Schnurle (1998), Oblique subduction of the Gagau Ridge beneath the Ryukyu accretionary wedge system: Insights from marine observations and sandbox experiment, *Mar. Geophys. Res.*, 20(5), 383–402.
- Frohlich, C., and S. D. Davis (1990), Single-link cluster analysis as a method to evaluate spatial and temporal properties of earthquake catalogs, *Geophys. J. Int.*, 100, 19–32.
- Gardner, J., and L. Knopoff (1974), Is the sequence of earthquakes in southern California, with aftershocks removed, Poissonian?, *Bull. Seismol. Soc. Am.*, 64, 1363–1367.
- Ho, C. S. (1979), Geologic and tectonic framework of Taiwan, *Mem. Geol. Soc. China*, 3, 57–72.
- Ho, C. S. (1986), A synthesis of the geologic evolution of Taiwan, *Tectonophysics*, 125, 1–16.
- Hsu, M. T. (1961), Seismicity of Taiwan (Formosa), *Bull. Earthquake Res. Inst. Univ. Tokyo*, 39, 831–847.
- Kagan, Y. (1991), Likelihood analysis of earthquake catalogues, *Geophys. J. Int.*, 106, 135–148.
- Kao, H., G. C. Huang, and C. S. Liu (2000), Transition from oblique subduction to collision in the northern Luzon arc-Taiwan region: Constraints from bathymetry and seismic observations, *J. Geophys. Res.*, 105(B2), 3059–3079.
- Lallemand, S., and C. S. Liu (1998), Geodynamic implications of present-day kinematics in the southern Ryukyus, *J. Geol. Soc. China*, 41, 551–564.
- Lallemand, S., C. Liu, S. Dominguez, P. Schnurle, and J. Malavieille (1999), Trench-parallel stretching and folding of forearc basins and lateral migration of the accretionary wedge in the southern Ryukyus: A case of strain partition caused by oblique convergence, *Tectonics*, 18(2), 231–247.

- Lewis, P. A. W., and E. Shedler (1979), Simulation of non-homogeneous Poisson processes by thinning, *Nav. Res. Logistics Q.*, 26, 403–413.
- McClay, K. R. (1992), Glossary of thrust tectonic term, in *Thrust Tectonics*, edited by K. R. McClay, pp. 419–433, CRC Press, Boca Raton, Fla.
- Mining Research and Service Organization (1982), Final report of SLAR survey of the Republic of China, 84 pp., Min. Res. and Serv. Org. of Ind. Technol. Res. Inst., Hsin Chu, Taiwan.
- Musmeci, F., and D. Vere-Jones (1992), A space-time clustering model for historical earthquakes, *Ann. Inst. Stat. Math.*, 44, 1–11.
- Ogata, Y. (1978), The asymptotic behavior of maximum likelihood estimators for stationary point processes, *Ann. Inst. Statist. Math.*, 30A, 243–261.
- Ogata, Y. (1981), On Lewis' simulation method for point processes, *IEEE Trans. Inf. Theory*, IT-27, 23–31.
- Ogata, Y. (1988), Statistical model for earthquake occurrences and residual analysis for point processes, *J. Am. Stat. Assoc.*, 83, 9–27.
- Ogata, Y. (1992), Detection of precursory relative quiescence before great earthquakes through a statistical model, *J. Geophys. Res.*, 97, 19,845–19,871.
- Ogata, Y. (1998), Space-time point-process models for earthquake occurrences, *Ann. Inst. Stat. Math.*, 50, 379–402.
- Ogata, Y. (2004), Space-time model for regional seismicity and detection of crustal stress changes, *J. Geophys. Res.*, 109, B03308, doi:10.1029/2003JB002621.
- Ogata, Y., and J. Zhuang (2005), Space-time ETAS models and an improved extension, *Tectonophysics*, in press.
- Ogata, Y., K. Katsura, and M. Tanemura (2003), Modelling heterogeneous space-time occurrences of earthquake and its residual analysis, *Appl. Stat. (J. R. Stat. Soc. Ser. C)*, 52, 499–509.
- Okada, Y. (1992), Internal deformation due to shear and tensile faults in a half-space, *Bull. Seismol. Soc. Am.*, 82, 1018–1040.
- Omori, F. (1894), On after-shocks of earthquakes, *J. Coll. Sci. Imp. Univ. Tokyo*, 7, 111–200.
- Parzen, E., K. Tanabe, and G. Kitagawa (Eds.) (1998), *Selected Papers of Hirotugu Akaike*, Springer, New York.
- Pelletier, B., and J. F. Stephan (1986), Middle Miocene obduction and late Miocene beginning of collision registered in the Hengchun peninsula: Geodynamic implications for the evolution of Taiwan, *Tectonophysics*, 125, 133–160.
- Rathbun, S. L. (1993), Modelling marked spatio-temporal point patterns, *Bull. Int. Stat. Inst.*, 55(2), 379–396.
- Rathbun, S. L. (1996), Asymptotic properties of the maximum likelihood estimator for spatio-temporal point processes, *J. Stat. Plan. Inference*, 51, 55–74.
- Resenberg, P. (1985), Second-order moment of central California Seismicity, 1969–1982, *J. Geophys. Res.*, 90(B7), 5479–5495.
- Sakamoto, Y., and H. Akaike (1978), Analysis of cross classified data by AIC, *Ann. Inst. Statist. Math.*, 30, 185–197.
- Schnurle, P., C. S. Liu, S. Lallemand, and D. Reed (1998), Structural controls of the Taitung Canyon in the Huatung Basin east of Taiwan, *Terr. Atmos. Oceanic Sci.*, 9, 453–473.
- Sun, S. C. (1963), The reef limestones and the geologic structures in the vicinity of Kaohsiung City, Taiwan, *Pet. Geol. Taiwan*, 2, 47–64.
- Sun, S. C. (1964), Photogeologic study of the Tainan-Kaohsiung coastal plain area, Taiwan, *Pet. Geol. Taiwan*, 3, 39–51.
- Suppe, J. (1980), Imbricated structure of western foothills belt, south-central Taiwan, *Pet. Geol. Taiwan*, 17, 1–16.
- Tsai, Y. B. (1985), A study of disastrous earthquakes in Taiwan, 1683–1895, *Bull. Inst. Earth Sci. Acad. Sin.*, 5, 1–44.
- Tsai, Y. B. (1986), Seismotectonics of Taiwan, *Tectonophysics*, 125, 17–37.
- Tsai, Y. B., T. L. Teng, J. M. Chiu, and H. L. Liu (1997), Tectonic implications of the seismicity in the Taiwan region, *Mem. Geol. Soc. China*, 2, 13–41.
- Utsu, T. (1969), Aftershock and earthquake statistics. I: Some parameters which characterize an aftershock sequence and their interrelations, *J. Fac. Sci., Hokkaido Univ., Ser. VII, Geophys.*, 3, 129–195.
- Wang, J. H. (1998), Studies of earthquake seismology in Taiwan during the 1897–1996 period, *J. Geol. Soc. China*, 41, 291–336.
- Wang, J. H., and H. C. Kuo (1995), A catalogue of  $M_S \geq 7$  Taiwan earthquakes (1900–1994), *J. Geol. Soc. China*, 38, 95–106.
- Yamanaka, Y., and K. Shimazaki (1990), Scaling relationship between the number of aftershocks and the size of the main shock, *J. Phys. Earth*, 38, 305–324.
- Yoshioka, S. (2001), Coseismic slip distribution of the 1999 Chi-Chi, Taiwan, earthquake deduced from inversion analysis of GPS data, *Bull. Seismol. Soc. Am.*, 91, 1182–1189.
- Yu, S. B., H. Y. Chen, and L. C. Kuo (1997), Velocity field of GPS stations in the Taiwan area, *Tectonophysics*, 274, 41–59.
- Zhuang, J., Y. Ogata, and D. Vere-Jones (2002), Stochastic declustering of space-time earthquake occurrences, *J. Am. Stat. Assoc.*, 97, 369–380.
- Zhuang, J., Y. Ogata, and D. Vere-Jones (2004), Analyzing earthquake clustering features by using stochastic reconstruction, *J. Geophys. Res.*, 109, B05301, doi:10.1029/2003JB002879.

C.-P. Chang, Center for Space and Remote Sensing Research, National Central University, Chung-Li, 320 Taiwan. (cpchang@csr.ncu.edu.tw)

Y.-I. Chen, Institute of Statistics, National Central University, Chung-li, 320 Taiwan. (ychen@stat.ncu.edu.tw)

Y. Ogata and J. Zhuang, Institute of Statistical Mathematics, 4-6-7 Minami-Azabu, Minato-Ku, Tokyo 106-8569, Japan. (ogata@ism.ac.jp; zhuangjc@ism.ac.jp)

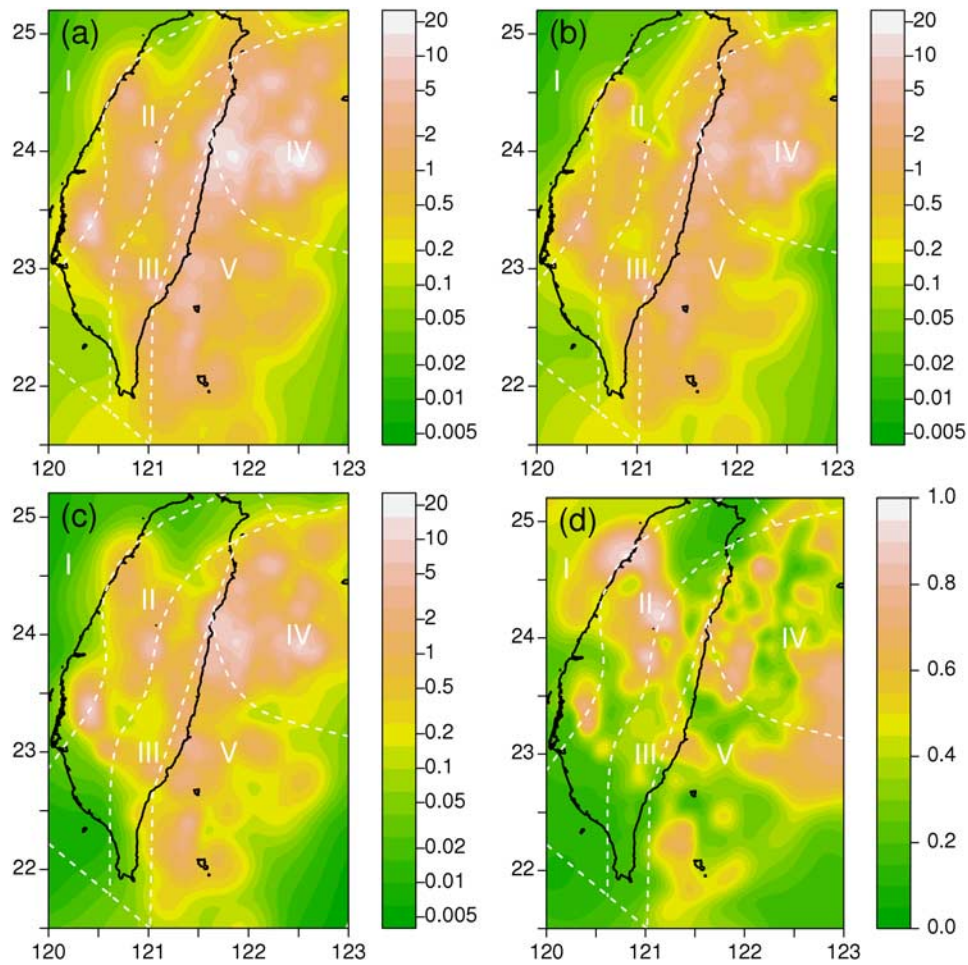


**Figure 3.** Estimated seismicity rates: (a) total seismicity rate  $\hat{m}(x, y)$ , (b) background seismicity rate  $\hat{\mu}(x, y)$ , (c) clustering seismicity rate  $\hat{C}(x, y)$ , and (d) clustering ratio  $\Omega(x, y)$ . See equations (20), (22), (24), and (25) for the definitions, respectively. The unit of the images for the rates in Figures 3a–3c is events/(degree<sup>2</sup> year). The uncertainty of the values of the clustering ratio at each location in Figure 3d can be roughly evaluated through the values of the total seismicity rate in Figure 3a or through the density of events in Figure 2a (see section 2.5).

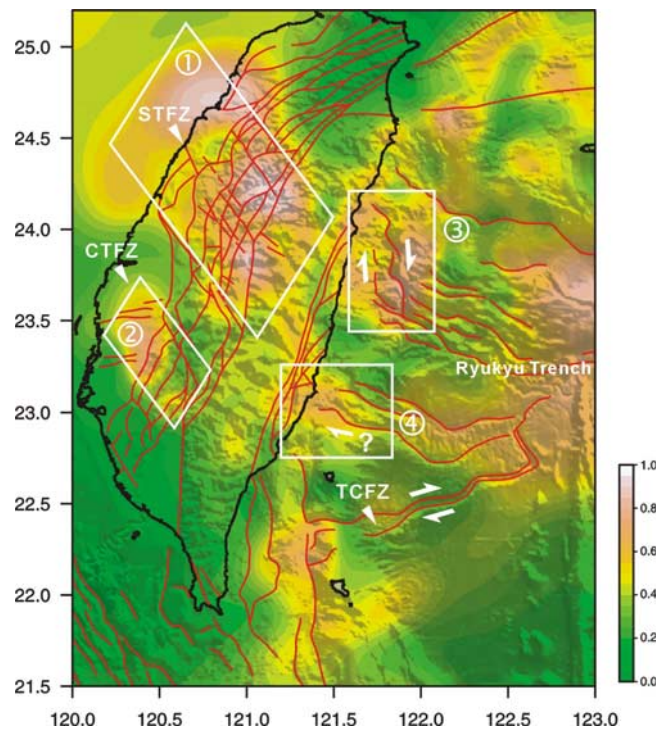


**Figure 4.** Distribution of seismic clustering ratio and structural interpretation of the Taiwan area. Surface faults are shown in solid lines as interpreted from multisources (data after *Mining Research and Service Organization* [1982], *Deffontaines et al.* [1994, 1997], *Lallemand and Liu* [1998], *Schnurle et al.* [1998], and *Kao et al.* [2000]). STFZ, Sanyi transfer fault zone; CTFZ, Chiayi transfer fault zone; TCFZ, Taitung Canyon Fault Zone. Details of the four areas with high clustering ratio (shown by white frames) are discussed in the text.

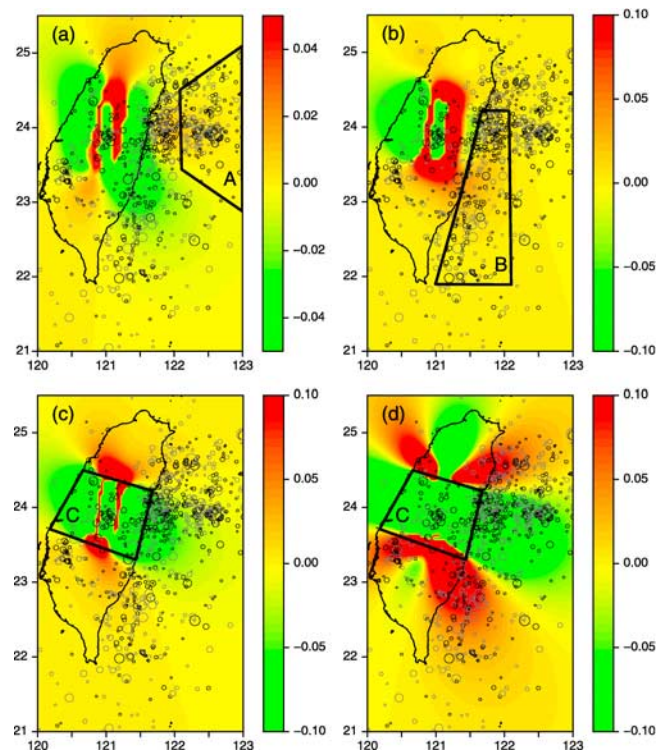


**Figure 5.** Distribution of  $\Delta\text{CFS}$  in the three typical seismic regions in Taiwan and its vicinity, caused by the assumed aseismic slip on the deeper part of the Chi-Chi earthquake fault (see text for the detail): (a) far offshore to the northeast of Taiwan Island (region A) at the depth of 30 km with receiver fault angles of (strike, dip, rake) = (270°, 30°, 90°); (b) eastern offshore region (region B) to the LV (Longitudinal Valley) at the depth of 25 km with receiver fault angles (10°, 30°, 60°); (c) central inland region (region C) at the depth of 15 km with receiver fault angles (10°, 30°, 60°); (d) central inland region (region C) as in Figure 5c, but with receiver fault angles (135°, 90°, 0°). The unit of the  $\Delta\text{CFS}$  is given in bars. The depths are chosen at which most earthquakes occur inside the corresponding regions.